

DFT Analysis of Structural, Electrical, and Optical Properties of S, Si, and F-Doped GeO₂ Rutile: Implications for UV-Transparent Conductors and Photodetection

Younes Ziat¹, Hamza Belkhanchi^{2*}, Zakaryaa Zarhri³.

^{1,2}Engineering and Applied Physics Team (EAPT), Superior School of Technology, Sultan Moulay Slimane University, Beni Mellal, Morocco.

^{1,2}The Moroccan Association of Sciences and Techniques for Sustainable Development (MASTSD), Beni Mellal, Morocco.

³SECIHITI- Faculty of Chemical Sciences and Engineering, The Autonomous University of Morelos State, Av Universidad 1001, C.P. 62209, Cuernavaca, Morelos, Mexico.

E-mail: ²hamzastudentestbm@gmail.com.

ARTICLE INFO.

Article history:

Received 5 Aug 2024

Received in revised form 8 Aug 2024

Accepted 21 Dec 2024

Available online 12 Jan 2025

KEYWORDS

GeO₂ Rutile; doped GeO₂; DFT;
Semiconductor; Optical properties.

ABSTRACT

This study examines the structural, electrical, and optical properties of S-, Si-, and F-doped GeO₂ rutile with a 6.25% doping concentration using density functional theory (DFT) and the FP-LAPW method. The results show that the structural parameters align with previous studies. Doping reduces the band gap from 4.09 eV for pure GeO₂ to 1.98 eV for GeO_{1.9375}Si_{0.0625}. The optical properties, including dielectric constant, conductivity, refractive index, and absorption spectrum, were analyzed up to 13 eV, revealing anisotropy along the zz (001) and xx (100) axes. These doped materials are promising for UV-sensitive photonic detectors, as they remain efficient even under sunlight exposure in the visible and infrared spectra. This could lead to the development of photodetection devices suitable for bright environments where traditional detectors are affected by sunlight.

*Corresponding author.

DOI: <https://doi.org/10.51646/jsesd.v14i1.232>

This is an open access article under the CC BY-NC license ([http://Attribution-NonCommercial 4.0 \(CC BY-NC 4.0\)](http://Attribution-NonCommercial 4.0 (CC BY-NC 4.0))).



تحليل الخصائص الهيكلية والكهربائية والبصرية لأوكسيد الجرمانيوم (GeO_2) في طور الروتيل المطعم بالكبريت (S)، والسيليكون (S) والفلور (F) باستخدام نظرية الكثافة الوظيفية (DFT): تطبيقات في الموصلات الشفافة للأشعة فوق البنفسجية والكشف الضوئي

يونس زيات، حمزة بلخشي، زكرياء زغري.

ملخص: تتبعت هذه الدراسة في الخواص الهيكلية والكهربائية والبصرية لروتيل GeO_2 المطعم بالكبريت، السيليكون والفلور المطعم بنسبة 6.25% باستخدام نظرية الكثافة الوظيفية (DFT) بواسطة تقنية FP-LAPW. أظهرت النتائج أن القيم البنيوية المحسوبة تتفق مع الأبحاث السابقة. وانخفضت طاقة الفجوة مع التطعيم من 4.09 eV ل GeO_2 الخالص إلى 1.98 eV ل $\text{GeO}_{1.9375}\text{Si}_{0.0625}$. تم تحليل الخواص الضوئية، مثل ثابت العزل الكهربائي، والتوصيلية، ومعامل الانكسار، ودالة الفقد، وطيف الامتصاص، وصولاً إلى طاقة فوتون 13 eV، مما يكشف عن تباين في محوري ZZ (001) و XX (100). هذه المواد المدعمة واعدة لاستخدامها في أجهزة الكشف الفوتوني الحساسة للأشعة فوق البنفسجية، حيث تظل فعالة حتى عند تعرضها لأشعة الشمس في الطيف المرئي والأشعة تحت الحمراء. قد يؤدي ذلك إلى تطوير أجهزة للكشف الضوئي مناسبة للبيئات الساطعة حيث تتأثر الأجهزة التقليدية بأشعة الشمس.

الكلمات المفتاحية: أكسيد الجرمانيوم في طور الروتيل، أكسيد الجرمانيوم المطعم، نظرية الكثافة الوظيفية، أشباه الموصلات، الخصائص البصرية.

1. INTRODUCTION

Ultra-wide bandgap semiconductors (bandgap larger than 3.4 eV) are extremely promising for high-power applications and deep-ultraviolet optoelectronics, thanks to their enhanced thermal robustness, their ability to tolerate intense electric fields, and their ability to operate at shorter wavelengths [1], these properties pave the way for new technological advances in these fields. Significant efforts have been invested in research into new ultra-wide bandgap semiconductor materials, with the aim of going beyond the performance of current materials and constantly improving devices. Nevertheless, doping must be used to control the majority carrier type in order to use materials in optoelectronics applications. However, doping semiconductor materials is a difficult task [2, 3, 4]. For instance, because dopant incorporation causes their formation energy to decrease linearly with fluctuations in the Fermi energy, native defects frequently passivate dopants in semiconductors [2]. Another significant issue for semiconductors is doping asymmetry [5]. It results from the fact that most semiconductors have high dopant ionization energies due to either a low valence-band maximum or a high conduction-band minimum compared to the vacuum level [3].

Germanium dioxide, also known as germanium IV oxide, is a chemical compound with the chemical formula GeO_2 , it's used in optical, electronic and semiconductor applications [6, 7, 8, 9], and with their unique properties of luminescence, catalysis and high surface area, it is used in physical and chemical applications [10, 11, 12]. Various methods can be used to manufacture it, including laser ablation [13], chemical reduction [14] and the hydrothermal process [15]. Germanium itself is a chemical element with atomic number 32 and belongs to the same family as carbon, silicon and tin in the periodic table of elements. Although germanium is not as abundant as silicon in the earth's crust, it has interesting semiconducting properties that make it a useful material for electronics [16, 17][18], the trigonal structure of α -quartz [19] and the amorphous glass [20, 21], each of these forms has specific properties and applications. In this paper, we present rutile germanium oxide ($r\text{-GeO}_2$) as a potentially useful material for ambipolar doping in ultrawide band-gap semiconductors. GeO_2 have rutile type structure that the most common MX2 structure and the electronic properties of this class of compounds vary widely from insulating to metallic behavior [22]. Numerous studies have been carried out using a variety of theoretical and experimental methods [23, 24, 25, 26]. The GeO_2 are large energy gap (E_g) semiconductors (4.44-

4.64 eV) [6, 5] with an appreciable degree of iconicity. Although there has been considerable debate over the years over the properties of the fundamental absorption edge GeO₂, the current experimental picture indicates that these compounds display a direct but optically forbidden fundamental gap at the center of the Brillouin zone [27]. The structural, electronic, and optical properties of GeO₂ have been investigated using a wide range of analytical techniques. These include use of the shell model and Buckingham potential with GULP computational package [28], application of the FP-LAPW method based on first principles [18], and application of the local density approximation (LDA) and generalized gradient approximation (GGA) [29].

Traditional doping methods have been explored with varying success, but the role of specific dopants like sulfur (S), silicon (Si), and fluorine (F) in modifying the material's behavior remains inadequately understood. Sulfur (S), Silicon (Si) and Fluorine (F), were chosen as dopants for their distinct electronic characteristics and their potential to significantly impact the electronic structure of GeO₂. Sulfur, for instance, can introduce localized states in the band gap, while silicon and fluorine are expected to influence the electronic conductivity and optical responses in unique ways.

By doping rutile GeO₂ with sulfur (S), Silicon (Si) and Fluorine (F), this study aims to understand how these impurities affect the crystal structure, electronic properties and optical characteristics of the material. The GGA and mBJ approach is used to obtain precise information on E_g, electronic energy levels and optical transitions. This research will help to shed light on the engineering possibilities of GeO₂ properties for various applications in the fields of electronics and optics.

2. METHOD CALCUL

Wien2k package was used to process the calculations of materials. It is particularly appreciated for its ability to use the Full Potential Linearized Plane Wave (FP-LAPW) method, which is based on Density Functional Theory (DFT) [30, 31, 32]. The DFT method using a generalized gradient approach (GGA), is an advanced and powerful approach for studying the electronic properties of GeO₂ doped with elements such as Sulfur (S), Silicon (Si) and Fluorine (F). In DFT-GGA, the basic DFT equations are solved using a GGA-type exchange-correlation functional, such as the Perdew-Burke-Ernzerhof (PBE) functional. This GGA functional improves the description of electronic properties over conventional DFT approaches by taking into account electron density gradients. Additionally, we made use of the modified Becke Johnson (mBJ) correlation potential [33], which allows us to optimize the corresponding potential for electronic band structure calculations. The total energy and charge convergence during self-consistent field (SCF) were fixed at 0.0001 (Ry) and 0.001 (e). The Brillouin zone is densely sampled with a mesh of 1000 k-points, employing octahedral integration.

To study GeO₂ doped with S, Si and F using the GGA-mBJ method, it is essential to specify the positions of the dopant atoms (S, Si and F) in the GeO₂ unit cell, see Figure 1. These doping atoms generally replace oxygen (O) atoms in the crystal structure, introducing defects into the crystal lattice and affecting the material's electron density.

To fully characterize the crystal lattice of GeO₂ doped with S, Si and F, it is also essential to determine the crystal space group in which the material lies. The rutile-like structure of doped GeO₂ generally belongs to the P42/mnm space group (space number 136), which defines the crystalline symmetries of the material. The valence electrons of Ge (4s², 4p²) and O (2s², 2p⁴) atoms are treated explicitly.

The crystal structure of GeO₂ rutile belongs to the orthorhombic crystal system. It has tetragonal D_{4h}^{14} symmetry and r-centered symmetry, which means that it has an inversion of center. Atomic positions in this structure are defined in terms of the *c/a* ratio and the internal parameter *u*. In rutile GeO₂, germanium cations (Ge) occupy octahedral sites and are located at positions (0, 0, 0)

and (0.5, 0.5, 5) in the fractional coordinates. Oxygen anions (O) occupy octahedron sites and are located at positions $\pm (u, u, 0)$ and $\pm (1/2+u, 1/2-u, 1/2)$, each cation has two anions at $d_1 = \sqrt{2ua}$ and $d_2 = \left[2\left(\frac{1}{2}-u\right)^2 + \left(\frac{c}{2a}\right)^2 \right]^{\frac{1}{2}} a$ [34]. We used for the calculations of GeO₂,

2x2x1 supercells of rutile GeO₂. A mesh of 10 x10 x10 was used for k point sampling in the first Brillouin zone for the calculations of GeO₂ unit cell, and for supercell calculations. The calculated bulk lattice constants of rutile GeO₂ are $a_0=b_0=4.45 \text{ \AA}$ and $c_0=2.92 \text{ \AA}$, these values compare favorably with the experimental results ($a_0=b_0=4.395 \text{ \AA}$ $c_0=2.86 \text{ \AA}$) [19], demonstrating the accuracy of the calculations and the reliability of the data obtained.

The use of the GGA-mBJ method improves the description of electronic energy levels, E_g and optical properties of GeO₂ material doped with S, Si and F. This advanced approach offers more accurate results for electronic properties, which is particularly important for understanding the electronic and optical behavior of doped GeO₂ material in various technological applications, such as electronic devices, solar cells and other optoelectronic components. Using this calculation method, it is possible to optimize the design of doped materials for specific applications.

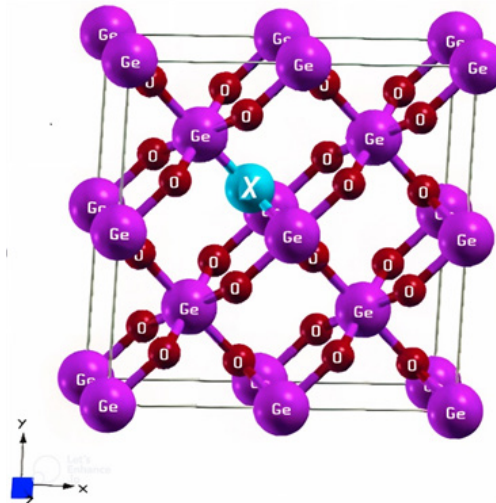


Figure 1. Structure of GeO_{1.9375}X_{0.0625} (X= S, Si and F).

3. ELECTRONIC PROPERTIES

The effect of O vacancies on the electronic and optical properties of GeO₂ is investigated by generating an O vacancy (VX) in the 2x2x1 supercell, leading to an X vacancy concentration of 6.25%. The total density of the states (TDOS) and corresponding partial density of the states (PDOS) for pure and (S, Si and F)-doped GeO₂ are shown in Figures 2, 3, 4 and 5.

The Figure 2 showing the pure structure of GeO₂ reveals that the valence band (VB), located between -10 eV and 0 eV, consists mainly of hybridized O-2p derivative states, with minor contributions from Ge-4p states. This observation suggests the predominance of covalent bonding in this energy region. On the other hand, the states near the bottom of the conduction band (CB), covering the energy range from 0 eV to 6 eV, are mainly made up of O-2p states. In general, the introduction of an O vacancy as a donor can potentially bring two additional electrons to the system, which can have a significant impact on its electronic properties.

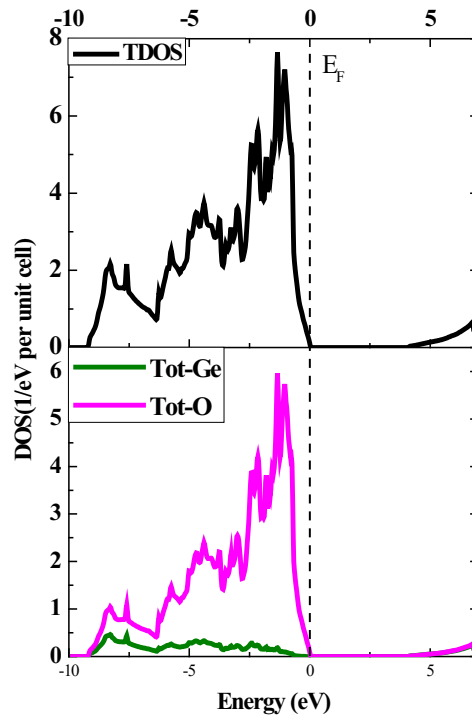


Figure 2. TDOS and PDOS of GeO₂ Pure.

Table 1. Eg value of r-GeO₂.

Method	Eg (eV)
DFT-LDA	1.80 [18]
	2.40 [37]
	3.12 [38]
DFT-GGA	1.25 [39]
	1.91 [35]
DFT-GGA + mbj (present work)	4.09
DFT-GGA + mbj	4.10 [35]
DFT-PAW + HSE06	4.64 [40]
DFT-LDA + G0W0	4.44 [6]
Experiment (UV-absorption)	4.68 [36]

For GeO₂, an unoccupied impurity state of the X vacancy appears in the bandgap, which does not destroy the semiconducting behavior but decreases the Eg. The calculated Eg value was 4.09 eV for GeO₂ pure, in agreement with ref [35], nevertheless, disagrees with the experimental ones of 4.68 eV [36].

In the doped structure, for GeO_{1.9375}S_{0.0625} (Figure 3) and GeO_{1.9375}Si_{0.0625} (Figure 4), the bottom of the valence band (VB) consists of O-2p and S-2p impurity states for GeO_{1.9375}S_{0.0625}, and impurity states O-2p and Si-2p for GeO_{1.9375}Si_{0.0625}, which are partially filled and can give rise to transitions between extrinsic states (S and Si) to allowed states below the Fermi level. The conduction level (CB) is dominated by impurity states Si-2p and Ge-4s in GeO_{1.9375}Si_{0.0625}.

In the GeO_{1.9375}F_{0.0625} doped structure (Figure 5), analysis shows that the bottom of the VB is mainly made up of O-2p impurity states, while the CB is mainly made up of F-2p and Ge-4s impurity states. These states can induce transitions between extrinsic fluorine (F) impurity energy levels and allowed states above the Fermi level. The presence of impurity levels alters the

electronic structure, shifting the Fermi level towards the CB, which is characteristic of n-type semiconductors. This suggests that electrical conductivity and bandgap width (E_g) are closely linked to the concentration of F in the material. The Burstein-Moss effect [41, 42] explains the widening of the E_g in the valence layer under the effect of F doping: by shifting the Fermi level into the conduction band (BC), impurity carriers fill this band, increasing the energy required for a photon to cause an electronic transition between the VB and an unoccupied state in the CB.

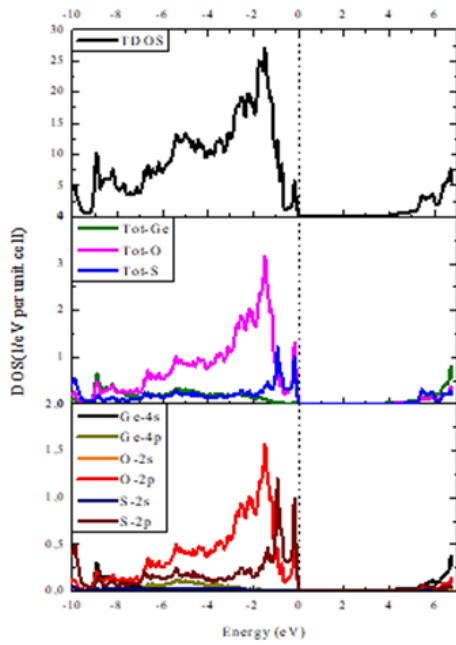


Figure 3. PDOS and TDOS of $\text{GeO}_{1.9375}\text{S}_{0.0625}$.

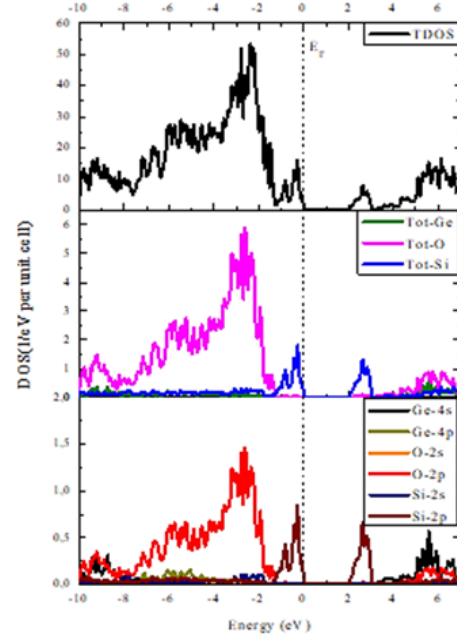


Figure 4. PDOS and TDOS of $\text{GeO}_{1.9375}\text{Si}_{0.0625}$.

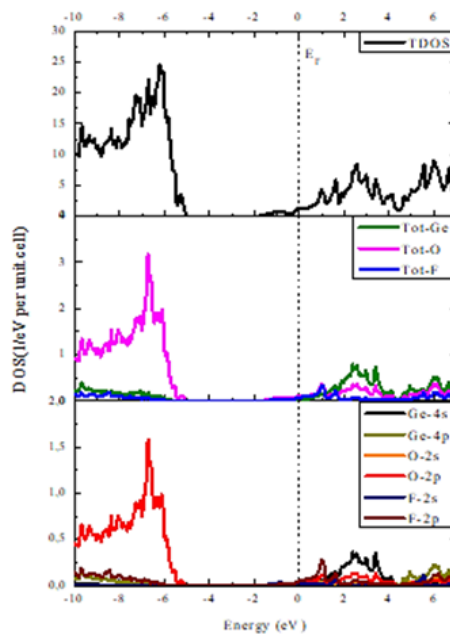


Figure 5. PDOS and TDOS of $\text{GeO}_{1.9375}\text{F}_{0.0625}$.

Dopants added to GeO_2 reduce the energy gap, making it easier for electrons to move from the VB to the CB. As a result, the energy gap is reduced from 4.09 eV for pure GeO_2 to 3.65 eV for $\text{GeO}_{1.9375}\text{S}_{0.0625}$, 3.23 eV for $\text{GeO}_{1.9375}\text{F}_{0.0625}$ and 1.98 eV for $\text{GeO}_{1.9375}\text{Si}_{0.0625}$. This enhances the

electrical conductivity of GeO₂ by modifying the Fermi levels, thus influencing the material's ability to conduct charges positively.

4. OPTICAL PROPERTIES

Electronic and structural properties are intimately related to optical qualities. Dielectric constant, conductivity, refractive index, loss function, and absorption spectrum are examples of optical properties that are connected to one another.

The dielectric function has the following possible notation:

$$\varepsilon(\omega) = \varepsilon_1(\omega) + i\varepsilon_2(\omega) \quad (1)$$

The complex dielectric function $\varepsilon(\omega)$ is a crucial tool for calculating the optical properties of materials. To obtain the imaginary part of this function, $\varepsilon_2(\omega)$, we used FP-LAPW calculations [43, 44]. This method allows us to apply the appropriate formula to extract the necessary data from our simulations. Thanks to this approach, we can better understand the behavior of light as it interacts with the material under study, which is essential for designing and optimizing optoelectronic devices.

$$\varepsilon_2(\omega) = \left(\frac{4\pi e^2}{\omega^2 m^2} \right) \sum \langle i | M | j \rangle^2 f_i (1 - f_j) \delta(E_f - E_i - \omega) d^3k \quad (2)$$

Where f_i is the Fermi distribution for the i th state, E_i is the energy of the electron in the state, m is the mass, M is the dipole matrix element, e is the electron charge, and i and j are the starting and final states, respectively. Using the Kramers-Kronig relation, we can immediately extract the $\varepsilon_1(\omega)$ from the $\varepsilon_2(\omega)$ as follows [45]:

$$\varepsilon_1(\omega) = 1 + \frac{2}{\pi} \int_0^\infty \left(\frac{\omega' \varepsilon_2(\omega')}{\omega'^2 - \omega^2} \right) \quad (3)$$

Once both the $\varepsilon_2(\omega)$ and the $\varepsilon_1(\omega)$ are calculated, all other optical characteristics, including absorption $\alpha(\omega)$, reflectivity $R(\omega)$, the refractive index $n(\omega)$, the complex conductivity function $\sigma(\omega)$ and the energy-loss spectrum $L(\omega)$ are described by expressions (4, 5, 6 and 7) [43, 46].

$$\alpha(\omega) = \sqrt{2}\omega \left[\sqrt{\varepsilon_1^2(\omega) + \varepsilon_2^2(\omega)} - \varepsilon_1(\omega) \right]^{\frac{1}{2}} \quad (4)$$

$$n(\omega) = \frac{1}{\sqrt{2}} \left[\sqrt{\varepsilon_1^2(\omega) + \varepsilon_2^2(\omega)} + \varepsilon_1(\omega) \right]^{\frac{1}{2}} \quad (5)$$

$$\sigma(\omega) = \sigma_1(\omega) + i\sigma_2(\omega) = -i \frac{\omega}{4\pi} [\varepsilon(\omega) - 1] \quad (6)$$

$$L(\omega) = \text{Im} \left(\frac{-1}{\varepsilon(\omega)} \right) = \frac{\varepsilon_2(\omega)}{\varepsilon_1^2(\omega) + \varepsilon_2^2(\omega)} \quad (7)$$

Figures 6-11 display the optical characteristics of both pure and GeO₂ doped materials. The $\varepsilon(\omega)$ obtained by utilizing zz directions (001) and xx directions (100) represents the system's linear reaction to an external electromagnetic field.

4.1. Dielectric function

The and real $\varepsilon_1(\omega)$ imaginary $\varepsilon_2(\omega)$ parts of the dielectric function calculated from (100) and (001) are shown in Figures 6 and 7, respectively. The values of the real parts $\varepsilon_1(0)$ are 0 eV for pure and doped GeO₂. After 0 eV, the ε_1 spectra increase with increasing energy. The values of $\varepsilon_1(\omega)$

at 12 eV becomes negative for pure and GeO₂ doped, which confirm the metallic characteristics of the compound [47]. The $\epsilon_2(\omega)$ has been calculated as a function of photon energy in Figure 7 and represents electron transitions between occupied VB states and unoccupied CB states. In this case, the behavior of the graph is described only by vertical transitions at the appropriate k value. The $\epsilon_2(\omega)$ is calculated from the electronic structure via the joint density of states and the momentum matrix elements between the occupied and unoccupied wave functions within the framework of the selection rules and is given by equation 2. Analysis of the $\epsilon_2(\omega)$ reveals the presence of various energy peaks, each with a particular significance in the context of our study. In structure (100), the most intense peak is observed, and it can be attributed to the interband transitions between the O-2p bands and the valence layer of our dopant. With the addition of the dopant, this peak shifts towards higher energies, reaching its maximum at an energy of 12 eV for a doping percentage of 6.25%. This shift towards higher energies suggests a broadening of the band gap for all doped structures. In structure (001), the most intense peak is associated with the F dopant and is described by the interband transitions between the O-2p and F-2p bands. This observation is consistent with the Burstein-Moss effect [41, 42], a phenomenon observed in heavily doped semiconductors.

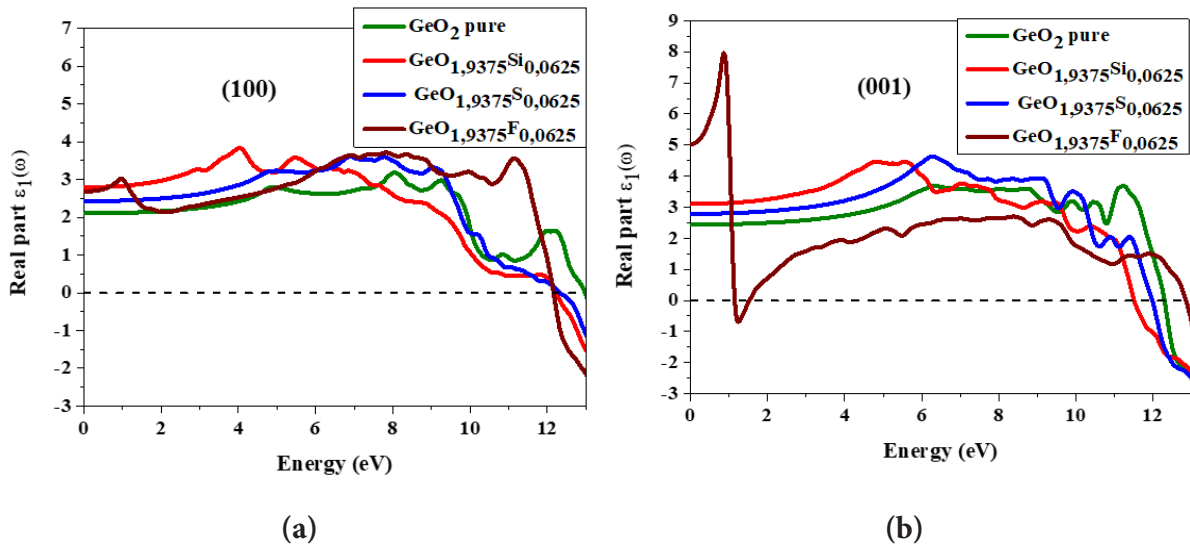


Figure 6. Real part versus energy of GeO_{1.9375}X_{0.0625} (X= S, Si and F) : a) position xx (100), b) position zz (001).

This effect is caused by the filling of the conduction level with impurity carriers from the dopant atoms, pushing the Fermi level into the conduction level, it's a critical phenomenon in heavily doped semiconductors, results from the occupation of low-energy states in the conduction band by excess carriers (electrons). In such cases, these states are no longer available for optical transitions, forcing the absorption edge to shift to higher energies. This shift manifests as an apparent widening of the material's band gap.

In the case of for GeO_{1.9375}F_{0.0625}, the Burstein-Moss effect plays a significant role in altering its electronic and optical properties. By introducing dopants, the carrier concentration increases significantly, leading to the filling of the conduction band states. This, in turn, raises the minimum energy required for electronic transitions from the valence band to the conduction band, effectively increasing the optical band gap observed in experimental measurements.

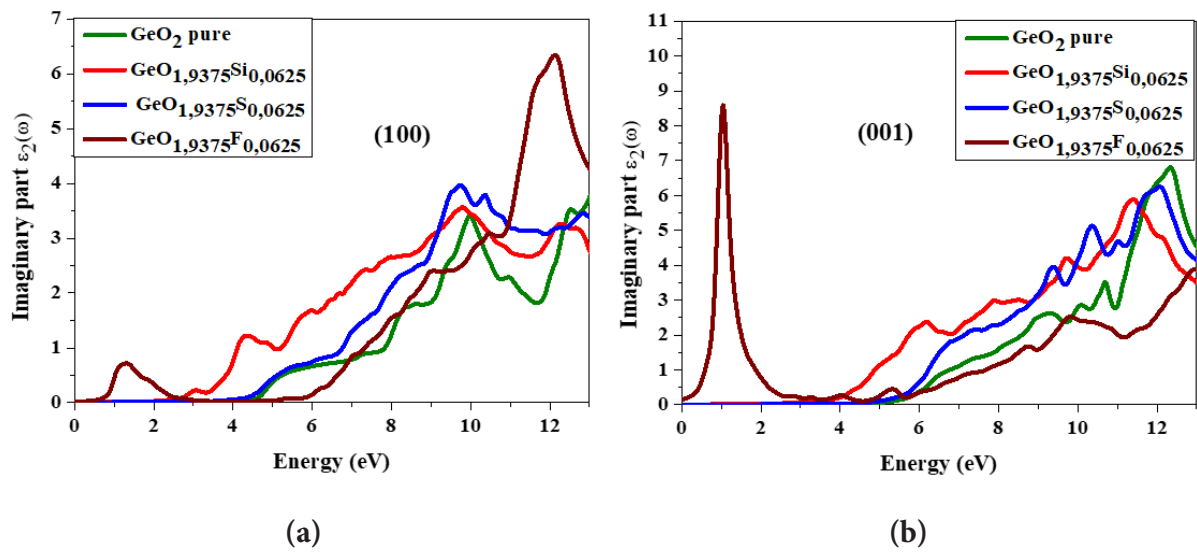


Figure 7. Imaginary part versus energy of GeO_{1.9375}X_{0.0625} (X= S, Si and F): a) position xx (100), b) position zz (001).

This redistribution of charge carriers increases the energy required for a photon to generate an electronic transition between the VB and an unoccupied state in the CB, thus explaining the rise in energies observed in the dielectric function peaks. In structure (100), data analysis reveals the presence of peaks in all doped structures, in the energy range from 4 to 13 eV. These peaks can be interpreted as electronic transitions in the band between the O-2p donor states and the unoccupied states located at the bottom of the conduction level, above the Fermi level. This observation suggests that electronic transitions to the conduction level are initiated from relatively low excitation energies. This feature also suggests an improvement in electrical conductivity compared with the pure structure. Indeed, electronic transitions from low energy levels can facilitate the movement of electric charges through the material, which is particularly advantageous for materials intended to be used as transparent conductors. Thus, these results suggest that doped structures present favorable characteristics for use in applications requiring both electrical conductivity and optical transparency.

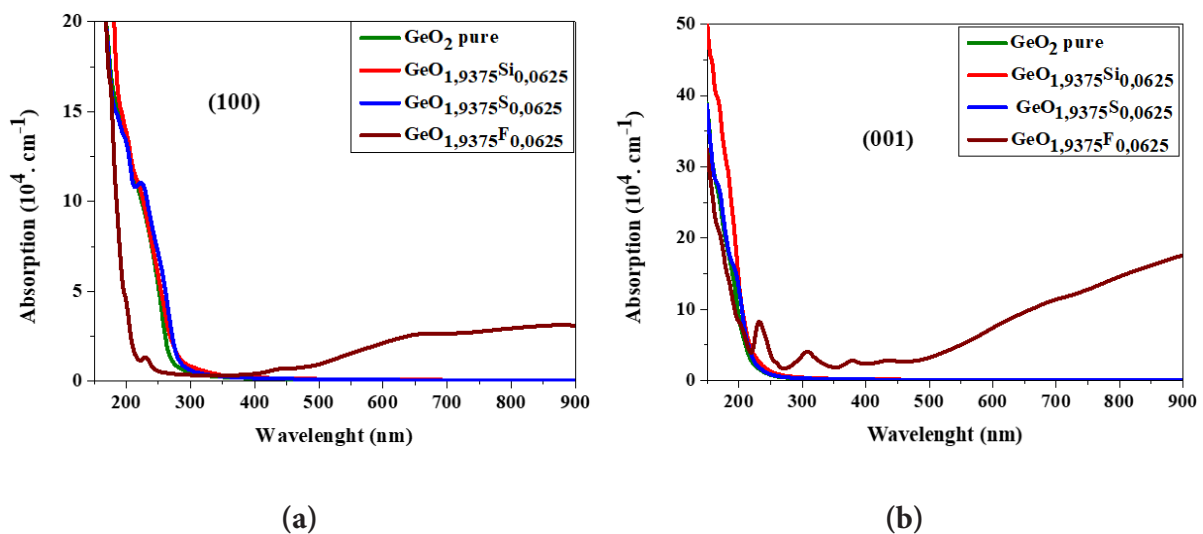


Figure 8. Absorption versus wavelength of GeO_{1.9375}X_{0.0625} (X= S, Si and F): a) position xx (100), b) position zz (001).

4.2. Absorption

Furthermore, Figure 8 shows that most of the absorption occurs in the ultraviolet region, while a smaller fraction is observed in the visible region. These results suggest that material F exhibits improved photocatalytic efficiency for visible light compared to pure GeO_2 (100). This observation is important in the context of photocatalytic application, as visible light constitutes a significant part of the available solar spectrum, and a material capable of efficiently absorbing this part of the spectrum may be more effective in converting light energy. Thus, these results suggest that $\text{GeO}_{1.9375}\text{F}_{0.0625}$ can offer significant advantages for photocatalytic applications involving the use of visible light.

4.3. Refractive index

Figure 9 shows the refractive index $n(\omega)$, the static refractive index has values of 1.45 and 1.55 from position (100) and (001), respectively, for pure GeO_2 . It then begins to increase with doping, reaching its maximum at 11.43 eV for the (100) direction and at 0.92 eV for the (001) direction with F doping. At this maximum, the refraction phenomenon disappears, as the $n(\omega)$ becomes almost equal to “1”, and the material behaves like a free space.

We note that the phenomenon of dispersion is very significant in the visible spectrum region. Due to this significant refractive index variation in the visible spectrum, the compound cannot be used in the fibre optics industry.

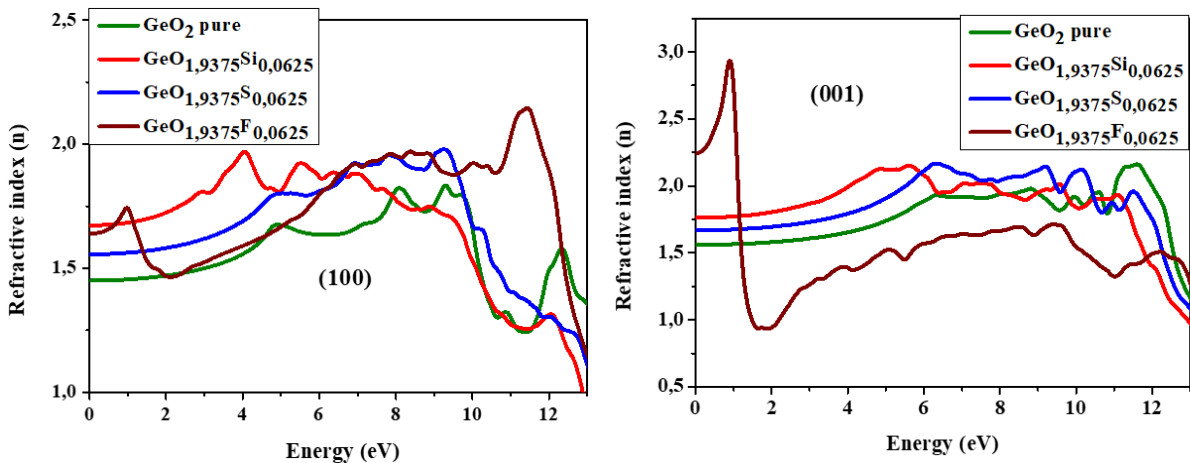


Figure 9. Refractive index versus energy of $\text{GeO}_{1.9375}\text{X}_{0.0625}$ ($\text{X} = \text{S}, \text{Si}$ and F):
a) position xx (100), b) position zz (001)

4.4. Optical conductivity

The optical conductivity corresponds to the electron conduction induced when a material is exposed to a photon of a specific frequency. Figure 10 illustrates the optical conductivity, $\sigma(\omega)$, for $\text{GeO}_{1.9375}\text{X}_{0.0625}$ ($\text{X} = \text{S}, \text{Si}$ and F) as a function of energy. Here, E_0 represents the initial absorption energy, the E_0 calculations in Table 2 depict the first two peaks and the maximum sigma value for GeO_2 pure and $\text{GeO}_{1.9375}\text{X}_{0.0625}$ ($\text{X} = \text{S}, \text{Si}$ and F).

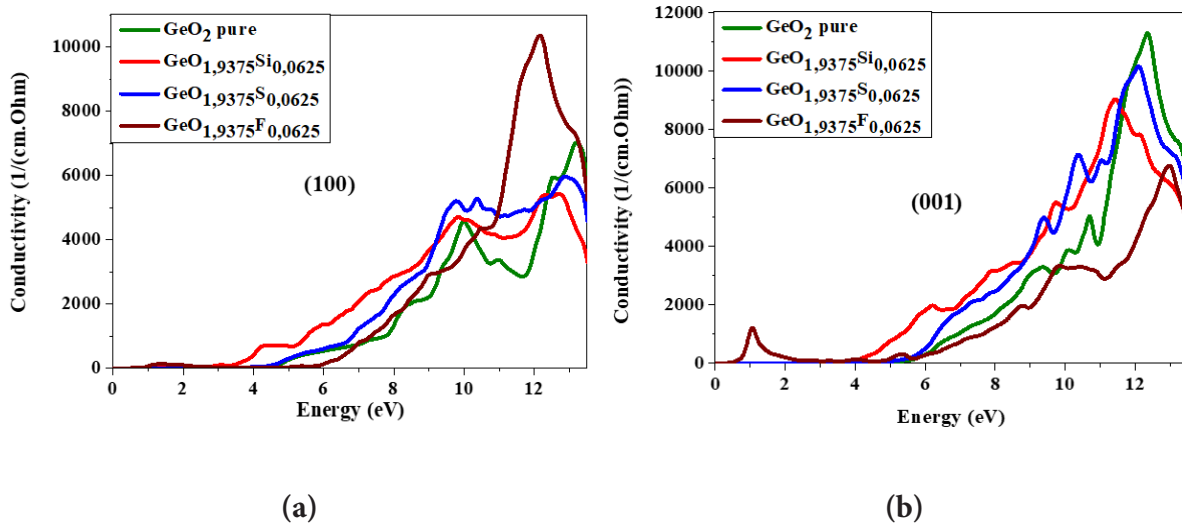


Figure 10. Conductivity versus energy of GeO_{1.9375}X_{0.0625} (X= S, Si and F): a) position xx (100), b) position zz (001).

In Figure 10, it is obvious that the compounds pure and doped GeO₂ exhibit high optical conductivity in ultraviolet range (3.8-13 eV). This observation suggests that pure and doped GeO₂ behaves as a semiconductor, and the optical conductivity phenomenon does not occur at a photon energy of 0 eV. The optical conductivity of the composite reflects the response to electromagnetic signals [48]. When exposed to an electric field, a sample demonstrates electrical conductivity, connecting the current density at its natural frequency. This conductivity is crucial for materials used in solar cells.

Table 2. E_0 calculations, the first two peaks and the maximum sigma value for GeO₂ pure and GeO_{1.9375}X_{0.0625} (X= S, Si and F).

Parameter-Direction	$E_0(eV)$	$E_1(eV)$	$E_2(eV)$	σ^{max} [1 / (Ohm.cm)]	
GeO ₂	xx	4.22	9.98	12.55	7121
	zz	5.15	9.35	10.09	11299
GeO _{1.9375} S _{0.0625}	xx	3.77	9.76	10.38	5972
	zz	4.92	9.39	10.37	10166
GeO _{1.9375} Si _{0.0625}	xx	2.71	9.82	12.43	5435
	zz	2.92	6.20	9.74	9049
GeO _{1.9375} F _{0.0625}	xx	5.11	12.5		10352
	zz	0.37	1.05	9.82	6764

4.5. Energy loss function

One excellent tool for examining the various characteristics of materials is the energy loss function $L(\omega)$ or Eloss. Apart from photon absorption, there are numerous different techniques to excite electrons in a material. For instance, a fast-moving electron might excite other electrons and lose energy represented by the Eloss when it travels through a material. Electrons in the solid are excited by energy, which is represented by the Eloss.

The Eloss spectrum is influenced by plasmonic excitations, intra- and inter-band transmissions, and other potential excitations. Thus, by examining the Eloss, which is connected to the dielectric function as seen below, all excitations can be found by equation 7.

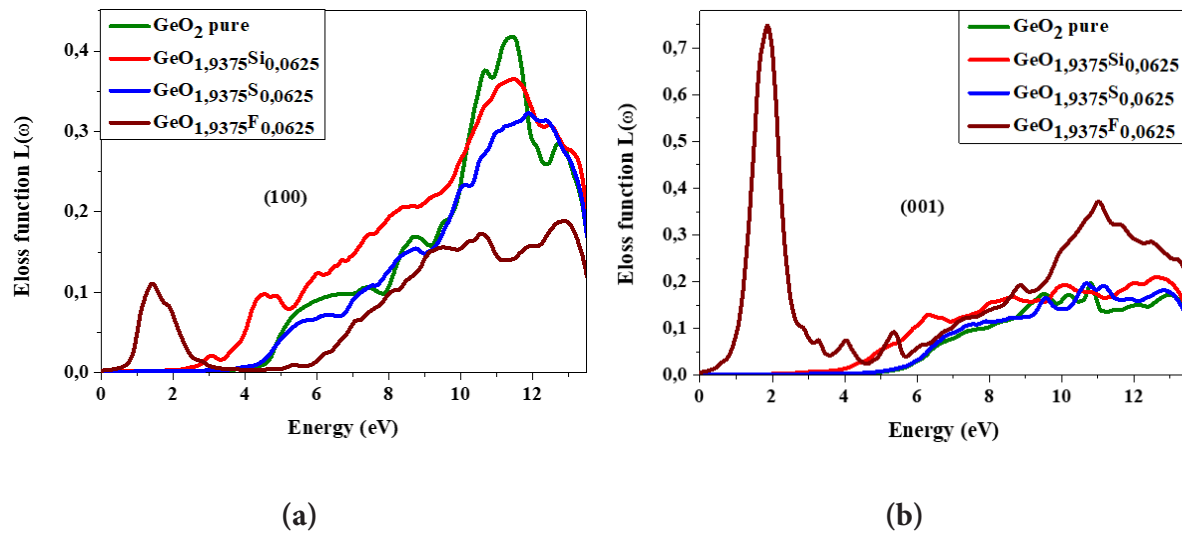


Figure 11. loss function versus energy of $\text{GeO}_{1.9375}\text{X}_{0.0625}$ (X= S, Si and F): a) position xx (100), b) position zz (001).

Eloss spectrum peaks can be attributed to interband transitions from the VB to the CB or to plasmons, which are collective oscillations of free electrons whose energy is dependent on the valence electron density. The intra- and inter-band excitations are associated with the peaks in the Eloss curves, the primary peak, shown in Figure 11, represents the energy of the plasmons of volume, which are polarized by electric fields in parallel (xx) and perpendicular (zz) directions. It is evident from both situations that the plasmonic frequency of GeO_2 compounds increases with thickness. Additionally, in the case of zz, $\text{GeO}_{1.9375}\text{F}_{0.0625}$ carbides have a greater plasmonic frequency than pure GeO_2 , in contrast to the xx case.

The anisotropy observed in the optical properties along the zz (001) and xx (100) axes has interesting implications for optoelectronic applications. This feature reveals a polarization-dependent optical response, which can be exploited in polarization-sensitive photodetectors. Such devices could offer enhanced performance in optical communication and imaging applications where detection of polarized light is essential. By aligning the material along the most reactive axis, such as zz (001), it would be possible to optimize detection. In solar cells, directional absorption plays a key role in energy conversion efficiency. Anisotropy would enable the material to be optimally oriented to maximize the absorption of incident light, taking into account its angle. This could also pave the way for the design of tandem solar cells where different layers exploit the anisotropic axes to cover a broader spectrum.

In this way, the anisotropy of optical properties is a strategic lever for designing high-performance optoelectronic devices. A better understanding and exploitation of this property could lead to significant advances in detection and energy conversion technologies.

5. CONCLUSION

In conclusion, calculations performed with Wien2k software, using the FP-LAPW method based on density functional theory (DFT) and the GGA-mBJ approach, have enabled in-depth study of the electronic and optical properties of GeO_2 doped with sulfur (S), silicon (Si) and fluorine (F). The use of the GGA-PBE exchange-correlation function, coupled with optimized calculations via the mBJ potential, has improved the description of electronic energy levels and optical properties, offering more accurate and relevant results for advanced technological applications. Analyses of the density of electronic states revealed marked differences in the behavior of doped

GeO₂, highlighting the impact of doping concentrations on the material's electronic properties. The effect of oxygen vacancies was also taken into account, showing significant changes in the electronic structure. Calculated optical properties, such as dielectric constant, refractive index and absorption spectrum, showed marked anisotropy, particularly in the zz and xx axes, which could have important implications for the design of UV-sensitive optoelectronic devices. Based on the calculated optical and electrical properties, we conclude that all the compounds studied are good candidates for applications in UV-sensitive photonic detectors, due to their ability to operate efficiently unaffected by sunlight in the visible and infrared spectrum. This phenomenon may open up prospects for photodetection devices in bright environments where sunlight could disrupt conventional detectors.

Author Contributions: Younes Ziat: Conceptualization (all authors wrote and contributed to the paper). Hamza Belkhanchi : Interpretation, writing, formal analysis, and investigation (all authors wrote and contributed to the paper). Zakaryaa Zarhri: Data curation and bibliographie (all authors wrote and contributed to the paper).

Funding statement: The authors are warmly grateful to the support of “The Moroccan Association of Sciences and Techniques for Sustainable Development (MASTSD), Beni Mellal, Morocco,” and to its president, professor Charaf Laghlimi, for the valuable proposals.

Data Availability Statement: Data is available on the request.

Conflicts of Interest: The authors declare that they have no conflict of interest.

Acknowledgments: The authors are warmly grateful to the support of “The Moroccan Association of Sciences and Techniques for Sustainable Development (MASTSD), Beni Mellal, Morocco,” and to its president, professor Charaf Laghlimi, for the valuable proposals. A special thank you to Professor Hanane Reddad from Sultan Moulay Slimane University, Beni Mellal, Morocco, for her technical and scientific support, as well as her full collaboration and discussion during the different steps of the present investigation.

REFERENCES

[1] J.Y. Tsao, S. Chowdhury, M.A. Hollis, D. Jena, N.M. Johnson, K.A. Jones, and J.A. Simmons, “Ultrawide-bandgap semiconductors: research opportunities and challenges”, *Advanced Electronic Materials*, vol. 4, no. 1, pp. 1600501, 2018.

[2] A. Walsh, J. Buckeridge, C.R.A. Catlow, A.J. Jackson, T.W. Keal, M. Miskufova, and A.A. Sokol, “Limits to doping of wide band gap semiconductors”, *Chemistry of Materials*, vol. 25, no. 15, pp. 2924-2926, 2013.

[3] Y. Yan and S.H. Wei, “Doping asymmetry in wide-bandgap semiconductors: Origins and solutions”, *physica status solidi (b)*, vol. 245, no. 4, pp. 641-652, 2008.

[4] W. Walukiewicz, “Intrinsic limitations to the doping of wide-gap semiconductors”, *Physica B: Condensed Matter*, vol. 302, pp. 123-134, 2001.

[5] S. Chae, J. Lee, K.A. Mengle, J.T. Heron, and E. Kioupakis, “Rutile GeO₂: an ultrawide-bandgap semiconductor with ambipolar doping”, *Applied Physics Letters*, vol. 114, no. 10, 2019.

[6] S. Chae, K.A. Mengle, K. Bushick, J. Lee, N. Sanders, Z. Deng, and E. Kioupakis, “Toward the predictive discovery of ambipolarly dopable ultra-wide-band-gap semiconductors: The case of rutile GeO₂”, *Applied Physics Letters*, vol. 118, no. 26, 2021.

[7] K.A. Mengle, S. Chae, and E. Kioupakis, “Quasiparticle band structure and optical properties of rutile GeO₂, an ultra-wide-band-gap semiconductor”, *Journal of Applied Physics*, vol. 126, no. 8, 2019.

[8] K. Bushick, K.A. Mengle, S. Chae, and E. Kioupakis, “Electron and hole mobility of rutile GeO₂ from first principles: An ultrawide-bandgap semiconductor for power electronics”, *Applied*

Physics Letters, vol. 117, no. 18, 2020.

[9] J.H. Sierra, D.O. Carvalho, L.R. Kassab, C.D. da Silva Bordon, R.E. Samad, N.U. Wetter, and M.I. Alayo, “Pedestal waveguides based on $\text{GeO}_2\text{-Bi}_2\text{O}_3$, $\text{GeO}_2\text{-PbO}$, Ta_2O_5 and SiO_xN_y cores as platforms for optical amplifiers, and nonlinear optics applications: Review of recent advances”, *Journal of Luminescence*, vol. 236, pp. 118113, 2021.

[10] M. Peng, X. Meng, J. Qiu, Q. Zhao, and C. Zhu, “ $\text{GeO}_2\text{: Bi, M}$ ($M = \text{Ga, B}$) glasses with super-wide infrared luminescence”, *Chemical Physics Letters*, vol. 403, no. 4-6, pp. 410-414, 2005.

[11] M. Seal, N. Bose, and S. Mukherjee, “Application of GeO_2 nanoparticle as electrically erasable memory and its photo catalytic behaviour”, *Materials Research Express*, vol. 5, no. 6, 065007, 2018.

[12] S.O. Kucheyev, T.F. Baumann, Y.M. Wang, T. van Buuren, J.F. Poco, J.H. Satcher, and A.V. Hamza, “Monolithic, high surface area, three-dimensional GeO_2 nanostructures”, *Applied Physics Letters*, vol. 88, no. 10, 2006.

[13] Y.H. Tang, Y.F. Zhang, N. Wang, I. Bello, C.S. Lee, and S.T. Lee, “Germanium dioxide whiskers synthesized by laser ablation”, *Applied Physics Letters*, vol. 74, no. 25, pp. 3824-3826, 1999.

[14] H. Yin, W. Xiao, X. Mao, H. Zhu, and D. Wang, “Preparation of a porous nanostructured germanium from GeO_2 via a “reduction–alloying–dealloying” approach”, *Journal of Materials Chemistry A*, vol. 3, no. 4, pp. 1427-1430, 2015.

[15] V.G. Hill and L.L. Chang, “Hydrothermal investigation of GeO_2 ”, *American Mineralogist: Journal of Earth and Planetary Materials*, vol. 53, no. 9-10, pp. 1744-1748, 1968.

[16] R. Pillarisetty, “Academic and industry research progress in germanium nanodevices”, *Nature*, vol. 479, no. 7373, pp. 324-328, 2011.

[17] C. Claeys and E. Simoen, “Germanium-based technologies: from materials to devices”, Elsevier, 2011.

[18] M. Sahnoun, C. Daul, R. Khenata, and H. Baltache, “Optical properties of germanium dioxide in the rutile structure”, *The European Physical Journal B-Condensed Matter and Complex Systems*, vol. 45, pp. 455-458, 2005.

[19] M. Grimsditch, A. Polian, V. Brazhkin, and D. Balitskii, “Elastic constants of $\alpha\text{-GeO}_2$ ”, *Journal of Applied Physics*, vol. 83, no. 6, pp. 3018-3020, 1998.

[20] B. Walker, C.C. Dharmawardhana, N. Dari, P. Rulis, and W.Y. Ching, “Electronic structure and optical properties of amorphous GeO_2 in comparison to amorphous SiO_2 ”, *Journal of Non-Crystalline Solids*, vol. 428, pp. 176-183, 2015.

[21] M. Micoulaut, L. Cormier, and G.S. Henderson, “The structure of amorphous, crystalline and liquid GeO_2 ”, *Journal of Physics: Condensed Matter*, vol. 18, no. 45, pp. R753, 2006.

[22] T. Yamanaka, J. Mimaki, and T. Tsuchiya, “The bond character of rutile type SiO_2 , GeO_2 and SnO_2 investigated by molecular orbital calculation”, *Zeitschrift für Kristallographie*, vol. 215, no. 7, 2000.

[23] L. Zhou and Z. Zhu, “Study of magneto-optical properties of $\text{GeO}_2\text{-B}_2\text{O}_3\text{-P}_2\text{O}_5\text{-ZnO-Tb}_2\text{O}_3$ glass doped with different rare-earth ions”, *Journal of Non-Crystalline Solids*, vol. 576, 121241, 2022.

[24] H.O. Tekin, L.R.P. Kassab, S.A. Issa, C.D. da Silva Bordon, M.S. Al-Buriahi, F.D.O.P. Delboni, and E.S. Magalhaes, “Structural and physical characterization study on synthesized tellurite (TeO_2) and germanate (GeO_2), glass shields using XRD, Raman spectroscopy, FLUKA and PHITS”, *Optical Materials*, vol. 110, 110533, 2020.

[25] D. Marrocchelli, M. Salanne, and P.A. Madden, “High-pressure behaviour of GeO_2 : a simulation study”, *Journal of Physics: Condensed Matter*, vol. 22, no. 15, 152102, 2010.

[26] G. Fraysse, A. Lignie, P. Hermet, P. Armand, D. Bourgogne, J. Haines, and P. Papet, “Vibrational origin of the thermal stability in the highly distorted α -quartz-type material GeO_2 : an

experimental and theoretical study”, *Inorganic Chemistry*, vol. 52, no. 12, pp. 7271-7279, 2013.

[27] Q.J. Liu, Z.T. Liu, L.P. Feng, and H. Tian, “First-principles study of structural, elastic, electronic and optical properties of rutile GeO₂ and α -quartz GeO₂”, *Solid State Sciences*, vol. 12, no. 10, pp. 1748-1755, 2010.

[28] E. Ghobadi and J.A. Capobianco, “Crystal properties of α -quartz type GeO₂”, *Physical Chemistry Chemical Physics*, vol. 2, no. 24, pp. 5761-5763, 2000.

[29] L. Giacomazzi and A. Pasquarello, “Vibrational spectra of vitreous SiO₂ and vitreous GeO₂ from first principles,” *Journal of Physics: Condensed Matter*, vol. 19, no. 41, pp. 415112, 2007.

[30] M. Orto, D. A. Pantazis, and F. Neese, “Density functional theory,” *Photosynthesis Research*, vol. 102, pp. 443-453, 2009.

[31] N. Argaman and G. Makov, “Density functional theory: An introduction,” *American Journal of Physics*, vol. 68, no. 1, pp. 69-79, 2000.

[32] P. Blaha, K. Schwarz, G. K. Madsen, D. Kvasnicka, and J. Luitz, *wien2k: An augmented plane wave + local orbitals program for calculating crystal properties*, vol. 60, no. 1, 2001.

[33] F. Tran and P. Blaha, “Accurate band gaps of semiconductors and insulators with a semilocal exchange-correlation potential,” *Physical Review Letters*, vol. 102, no. 22, pp. 226401, 2009.

[34] J. Robertson, “Electronic structure of SnO₂, GeO₂, PbO₂, TeO₂, and MgF₂,” *Journal of Physics C: Solid State Physics*, vol. 12, no. 22, pp. 4767, 1979.

[35] H. Singh, M. Singh, S. Kumar, and M. K. Kashyap, “Full potential calculation of electronic properties of rutile RO₂ (R=Si, Ge, Sn, and Pb) compounds via modified Becke-Johnson potential,” *Physica B: Condensed Matter*, vol. 406, no. 20, pp. 3825-3830, 2011.

[36] M. Stapelbroek and B. D. Evans, “Exciton structure in the UV-absorption edge of tetragonal GeO₂,” *Solid State Communications*, vol. 25, no. 11, pp. 959-962, 1978.

[37] D. M. Christie and J. R. Chelikowsky, “Electronic and structural properties of germania polymorphs,” *Physical Review B*, vol. 62, no. 22, pp. 14703-14711, 2000.

[38] C. Sevik and C. Bulutay, “Theoretical study of the insulating oxides and nitrides: SiO₂, GeO₂, Al₂O₃, Si₃N₄, and Ge₃N₄,” *Journal of Materials Science*, vol. 42, pp. 6555-6565, 2007.

[39] Q.-J. Liu, Z.-T. Liu, L.-P. Feng, and H. Tian, “First-principles study of structural, elastic, electronic, and optical properties of rutile GeO₂ and α -quartz GeO₂,” *Solid State Sciences*, vol. 12, no. 10, pp. 1748-1755, 2010.

[40] S. Chae, J. Lee, K. A. Mengle, J. T. Heron, and E. Kioupakis, “Rutile GeO₂: An ultrawide-band-gap semiconductor with ambipolar doping,” *Applied Physics Letters*, vol. 114, no. 10, pp. 102104, 2019.

[41] M. Feneberg, S. Osterburg, K. Lange, C. Lidig, B. Garke, R. Goldhahn, and al., “Band gap renormalization and Burstein-Moss effect in silicon- and germanium-doped wurtzite GaN up to 10²⁰ cm⁻³,” *Physical Review B*, vol. 90, no. 7, pp. 075203, 2014.

[42] P. V. Kamat, N. M. Dimitrijevic, and A. J. Nozik, “Dynamic Burstein-Moss shift in semiconductor colloids,” *The Journal of Physical Chemistry*, vol. 93, no. 8, pp. 2873-2875, 1989.

[43] Y. Ziat, A. Abbassi, A. Slassi, M. Hammi, A. A. Raiss, O. E. Rhazouani, and A. E. Kenz, “First-principles investigation of the electronic and optical properties of Al-doped FeS₂ pyrite for photovoltaic applications,” *Optics and Quantum Electronics*, vol. 48, no. 1, pp. 1-8, 2016.

[44] Y. Ziat, Z. Zarhri, H. Belkhanchi, O. Ifguis, A. D. Cano, and C. Lazrak, “Effect of Be and P doping on the electron density, electrical and optoelectronic conduct of half-Heusler LiMgN within ab initio scheme,” *Physica Scripta*, vol. 97, no. 10, pp. 105802, 2022.

[45] Y. Ziat, Z. Zarhri, M. Hammi, H. Belkhanchi, O. Ifguis, A. D. Cano, and A. C. Bastos, “Effect of (Na, Si, Al, K or Ca) doping on the electronic structure and optoelectronic properties of half-Heusler LiMgN alloy: Ab initio framework,” *Solid State Communications*, vol. 343, pp. 114665, 2022.

- [46] M. Radjai, A. Bouhemadou, and D. Maouche, "Structural, elastic, electronic, and optical properties of the half-Heusler ScPtSb and YPtSb compounds under pressure," *Condensed Matter Physics*, vol. 24, no. 4, 2021.
- [47] S. Mubashir, M. K. Butt, M. Yaseen, J. Iqbal, M. Iqbal, A. Murtaza, and A. Laref, "Pressure induced electronic, optical, and thermoelectric properties of cubic BaZrO₃: A first principle calculation," *Optik*, vol. 239, pp. 166694, 2021.
- [48] M. N. Islam and J. Podder, "Semiconductor to metallic transition in double halide perovskites Cs₂AgBiCl₆ through induced pressure: A DFT simulation for optoelectronic and photovoltaic applications," *Heliyon*, vol. 8, no. 8, 2022.